Z. Phys. B – Condensed Matter 47, 103–113 (1982)

Condensed
Zeitschrift für Physik B Matter

Experimental Study of the Amorphous Phases of Group-IV Semiconductors by the ^{119m}Sn Mössbauer Probe

L.K. Nanver*, G. Weyer, and B.I. Deutch
Institute of Physics, University of Aarhus, Denmark

Received January 7, 1982

The amorphous phases of silicon, germanium, and α-tin have been studied by Mössbauer emission spectroscopy on ion-implanted, radioactive ^{119m}Sn. Amorphous samples have been produced by ion implantations of various elements and by vacuum-evaporation techniques. The same well-defined type of complex spectrum is observed for all investigated amorphous samples. These spectra are characterized by an increase in average isomer shift of (0.15 ± 0.03) mm/s, a line broadening of $20 \pm 2\%$, and the same Debye temperature as compared with spectra of substitutional Sn in the respective crystalline host lattices. The spectra are proposed to originate from Sn atoms incorporated substitutionally in the amorphous host with distorted local surroundings. The recrystallization of the amorphous phase upon thermal and laser annealing has been monitored. After appropriate annealing, spectra characteristic of crystalline materials are observed for most samples. An exception are high-dose, inert-gas implanted samples where different complex defects seem to be formed in the annealing process.

I. Introduction

The amorphous phases of silicon and germanium have been a subject of extensive research, and numerous experimental methods have been employed [1], among others x-ray diffraction, Rutherford backscattering, electron microscopy, electron-spin-resonance and various electrical measurements. From these experiments information has been obtained on the basic structure and the macroscopic composition of the amorphous phase, as well as on electronic structure and lattice dynamics.

In this study Mössbauer spectroscopy on the 24-keV γ-radiation of ion-implanted ^{119m}Sn impurity atoms is explored as an alternative method of examining the amorphous phases of these semiconductors. Tin impurity atoms have previously been demonstrated to be useful probes in crystalline silicon and germanium. With this probe the electronic structure of the isoelectronic impurities was found to be very similar to that of the host crystal atoms [2] and the vibrational properties of the tin atoms appeared to be sensitive to details of the phonon density of states of the host lattices [3]. Radiogenic ^{119}Sn probe atoms introduced by ion implantations of different parent isotopes have also been utilized to investigate the structure of complex tin-impurity defects created by the implantation into these semiconductors [4, 5]. For a review of applications of Mössbauer spectroscopy to other amorphous materials, see [6].

Previously it has been shown that the amorphization of crystalline silicon by ion implantation of tin atoms yields a Mössbauer spectrum which was broader and shifted in position as compared to the single-line spectrum of substitutional tin in crystalline silicon [7]. The purpose of the present study, first and foremost, is to determine the origin of these deviations, i.e., whether these effects are due to properties specific to the tin-impurity atoms or whether and in what way they reflect properties of the amorphous host.

To distinguish influences on the spectra from the tin probe atoms and the host, extensive studies of the amorphous silicon phase have been undertaken, both as a function of the method of preparation and of

* Present address: ENST, Dept. Electronique et Physique, 46, Rue Barrault, F-75643 Paris, France

0722-3277/82/0047/0103/$02.20

any subsequent recrystallization. The results for cases considered to be characteristic of the amorphous phase of the host are compared to measurements of similarly prepared amorphous germanium and α-tin.

II. Experimental Procedures

Amorphous silicon and germanium films were prepared by evaporation onto quartz-glass plates. Conventional evaporation technique was employed with a pressure of $\sim 10^{-6}$ torr and evaporation rates of $\sim$100–250 Å/s. Films of about $3\text{–}4 \cdot 10^3$ Å thick were produced. Single crystals of α-tin were grown by a precipitation technique from a tin-mercury alloy [8].

Single crystals of *n*-type silicon and germanium, cut perpendicular to the ⟨111⟩ or ⟨100⟩ axes, were amorphized by ion implantation. With an isotope separator, various ions were implanted at energies of 10–90 keV and swept over an area $\sim 1\,\text{cm}^2$. The energies of the different isotopes were chosen in such a way that a maximum overlap of the different range distributions was achieved.

Similarly the ^{119m}Sn Mössbauer probe atoms were introduced by ion implantation into the various amorphous host materials. Mössbauer emission spectra of the thus produced samples were measured by resonance-counting technique [9]. Single-line $BaSnO_3$ or $CaSnO_3$ absorber material and quadrupole-split SnO_2 material were used in resonance detectors of the parallel-plate avalanche counter type. All isomer shifts are given with respect to SnO_2.

III. Experimental Results and Data Treatment

A. The Shape of the Amorphous Spectra

A series of silicon and germanium crystals were implanted at room temperature with a variety of elements at doses that considerably exceeded the amounts reported to give total amorphization of the implanted area ($\sim 10^{15}/\text{cm}^2$ for light-ion implants and $\sim 10^{14}/\text{cm}^2$ for heavy-ion implants, see for example [10]). A list of samples and their implantation conditions is presented in Table 1, which also includes ^{119m}Sn implantations into vapour deposited silicon and germanium films and into α-tin single crystals.

Using SnO_2 absorber material, the silicon and germanium samples were measured at both room temperature and liquid-nitrogen temperature. Despite the diversity of sources, the spectra all exhibit a similar intensity distribution. As will be discussed in Sect. IV, these spectra are typical for amorphous silicon and germanium and are therefore in the following referred to as the *a*-Si and *a*-Ge spectra. Examples of these spectra are shown in Fig. 1, where the spectra of ^{119}Sn in the respective crystalline materials (solid lines) are drawn in for comparison. The latter will be referred to as *c*-spectra. They have been interpreted as originating from Sn located substitutionally in the undisturbed crystalline matrix,

Table 1. List of implanted amorphous samples

Substrate	Sample no.	Substrate temp.	Ion	Implantation parameters	
				Dose (cm^{-2})	Energy (keV)
	Si1	RT	^{119}Sn	10^{15}	90
	Si2	RT	^{119}Sn	$5 \cdot 10^{14}$	60
		RT	^{118}Sn	10^{16}	60
	Si3	RT	^{30}Si	10^{16}	30
		RT	^{119}Sn	10^{14}	90
	Si4	450 °C	^{119}Sn	$5 \cdot 10^{14}$	90
		RT	^{20}Ne	10^{16}	30
Si⟨111⟩	Si5	450 °C	^{119}Sn	$5 \cdot 10^{14}$	90
		RT	^{20}Ne	$2 \cdot 10^{16}$	30
	Si6	450 °C	^{119}Sn	$5 \cdot 10^{14}$	90
		RT	^{84}Kr	$8 \cdot 10^{15}$	90
	Si7	RT	^{1}H	$5 \cdot 10^{16}$	10
		RT	^{119}Sn	10^{15}	60
	Si8	RT	^{16}O	$5 \cdot 10^{15}$	20
		RT	^{119}Sn	$5 \cdot 10^{14}$	90
	Si9	450 °C	^{119}Sn	$5 \cdot 10^{14}$	90
		RT	^{16}O	$5 \cdot 10^{15}$	20
	Si10	RT	^{119}Sn	10^{15}	90
Si⟨100⟩	Si11	RT	^{119}Sn	$5 \cdot 10^{14}$	60
		RT	^{118}Sn	10^{16}	60
	Si12	RT	^{64}Ge	10^{16}	48
		RT	^{119}Sn	10^{14}	60
Si films	Si13	RT	^{119}Sn	10^{14}	60
LN deposited	Si14	RT	^{119}Sn	10^{14}	60
RT deposited	Si15	RT	^{119}Sn	10^{15}	60
	Si16	RT	^{119}Sn	10^{16}	60
	Ge1	350 °C	^{119}Sn	$5 \cdot 10^{14}$	60
		RT	^{74}Ge	10^{16}	48
Ge⟨111⟩	Ge2	RT	^{74}Ge	10^{16}	48
		RT	^{119}Sn	$2 \cdot 10^{14}$	60
	Ge3	RT	^{119}Sn	10^{15}	60
	Ge4	RT	^{119}Sn	10^{15}	60
Ge films	Ge5	RT	^{119}Sn	10^{14}	60
RT deposited	Ge6	RT	^{119}Sn	10^{15}	60
α-Sn single crystals	α-Sn1	RT	^{119}Sn	$5 \cdot 10^{14}$	80
	α-Sn2	LN	^{119}Sn	$5 \cdot 10^{14}$	80
	α-Sn3	LN	^{118}Sn	10^{16}	80

Table 2. Mössbauer parameters of *c*- and *a*-spectra of Si, Ge, and α-tin. (IS = isomer shift, Γ_0 = natural linewidth, Γ_a = spectral half-width)

	c-Si	*c*-Ge	*c*-(α-Sn)
IS(RT) (mm/s)	1.76±0.02	1.86±0.02	2.03 ±0.02
IS(LN) (mm/s)	1.82±0.02	1.92±0.02	2.10 ±0.02
f(RT)	0.34±0.02	0.23±0.02	0.133±0.006
f(LN)	0.75±0.04	0.70±0.04	0.525±0.018
θ_D(K)	226 ±5	190 ±10	163 ±5
	a-Si	*a*-Ge	α-Sn[a]
IS(RT) (mm/s)	1.89±0.02	2.00±0.02	2.14±0.04
Γ_a/Γ_0	1.23±0.03	1.24±0.03	1.28±0.05
f(RT)	0.34±0.03	0.24±0.03	–
f(LN)	0.75±0.04	0.70±0.04	0.50±0.05
θ_D(K)	224 ±4	195 ±10	–

[a] sample α-Sn1 in Table 1

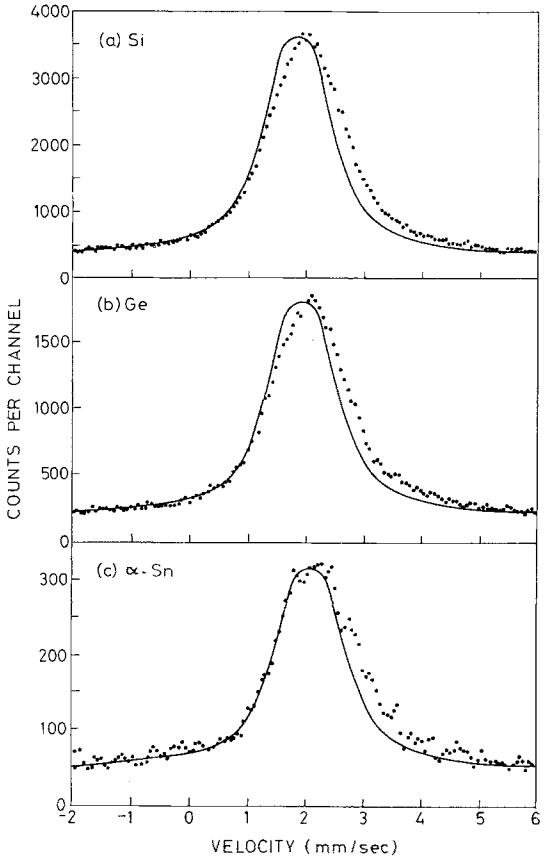

Fig. 1a–c. Mössbauer spectra (measured at liquid nitrogen temperature, SnO_2 absorber) of ^{119}Sn in amorphorized **a** silicon and **b** germanium and **c** α-tin (sample α-Sn1 in Table 1). The solid lines represent the spectra of the respective crystalline material

since only a single unbroadened emission line is observed [2, 3]. The Mössbauer parameters of this line are therefore obtained from a least-squares fit of the data to one Lorentzian emission line and the results are given in Table 2.

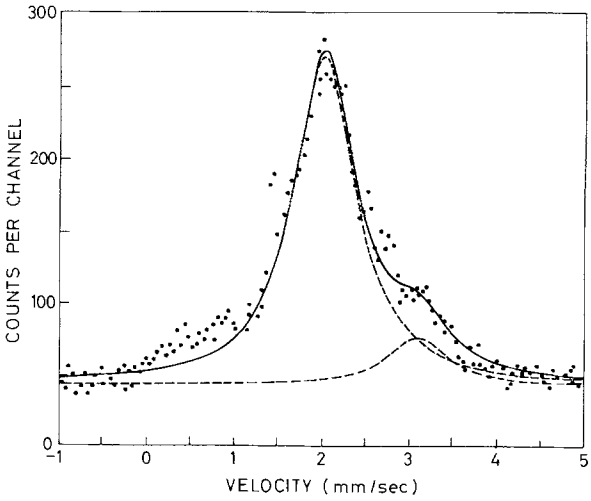

Fig. 2. Mössbauer spectrum (measured at liquid nitrogen temperature, $CaSnO_3$ absorber) of ^{119}Sn in α-Sn (sample α-Sn2 in Table 1)

Relative to their corresponding *c*-spectra, the *a*-spectra of silicon and germanium are seen to be very similar. They both exhibit a line broadening of 20 ±2% and an increase in average isomer shift of (0.15±0.03) mm/s, with respect to the *c*-spectra. Also the peak of an *a*-spectrum is pointed instead of flat as in the *c*-spectrum, indicating that it probably consists of a sum of lines with different isomer shifts, which are predominantly larger than that of the *c*-spectra.

The situation for α-tin is more complicated. Samples implanted at room temperature with ^{119}Sn to a dose of $5 \cdot 10^{14}$/cm^2 show two types of spectra. One type resembles the *a*-Si and *a*-Ge spectra, and an example is shown in Fig. 1c. The Mössbauer parameters of this spectrum are also included in Table 2. In other cases the line broadening and isomer-shift increase of this spectral type is less pronounced, perhaps indicating an incomplete amorphization of the implanted layer. Also, no spectrum shows a clear peaking as seen for the *a*-Si and *a*-Ge spectra. The other type of α-tin spectra observed can be fitted by a *c*-(α-tin) line plus a line at approximately 3 mm/s with an intensity of ~15%. An example is shown in Fig. 2. This type of spectrum was also observed for an implanted dose of 10^{16} Sn/cm^2.

An analysis of the *a*-spectra is not straightforward as individual components are completely unresolved and their intensities have the same temperature dependence (see Sect. IV.B). Some samples were measured with a $BaSnO_3$ resonance counter, which has a single resonance line. This did not give additional information, but the same line broadenings and average isomer shifts as for measurements with the SnO_2 counter.

However, the requirement that both the $BaSnO_3$- and SnO_2-absorber spectra have to be fitted with the same emission-line distribution will give some restriction on the number of fit possibilities. Attempts to fit the spectra with independent lines showed that at least four lines must be employed to give reasonable fits to the spectra. The largest restriction is given by the sharp peak of the SnO_2 spectra. Such peaks, which are slimmer than the spectrum of a single emission line (quadrupole-split by the absorber), are characteristic of a summation of individual components of lines (all quadrupole-split by the absorber). Fits of the *a*-spectra with up to 8 (quadrupole-split) lines show that multiline fits do reproduce the sharply peaked structure. Therefore, it is proposed that the *a*-spectra consist of a continuous distribution of lines. However, since no connection can be extracted from the present data between the isomer shifts, line intensities, or possible quadrupole splittings of these lines, only qualitative average properties of the line distributions (cf. Table 2) will be considered in the following.

B. The Temperature Dependence of the Amorphous Spectra

The temperature dependence of both the average isomer shift and the total spectral intensity of the amorphous spectra have, for selected silicon samples, been measured in the temperature interval 77–300 K. All measurements were made on the same experimental setup so that the relative isomer shifts from spectra to spectra are well determined. The quantity compared, the average isomer shift, is calculated as follows:

$$\delta_{av} = \Sigma\{N(v) - N(\infty)\} \cdot v / \Sigma\{N(v) - N(\infty)\} \quad (1)$$

where the sum is taken over the experimental velocity range, $N(v)$ is the number of counts at velocity v and $N(\infty)$ is the number of counts from all non-resonant events. No isomer-shift differences other than those expected from the second-order Doppler shift were observed.

When determining the intensity of the spectra, the crucial point is the determination of the normalization factor, $N(\infty)$, which cannot be derived with sufficient accuracy from a fit since no correct fit of the *a*-spectra is known. However, both the average isomer-shift measurements and a direct comparison of the shape of the spectra substantiate that there is no difference in the temperature dependences of the individual components. This fact is utilized to minimize the uncertainty of the relative intensities, in that it is then sufficient to compare the resonant areas relative to each other after the same background-substraction procedure has been applied.

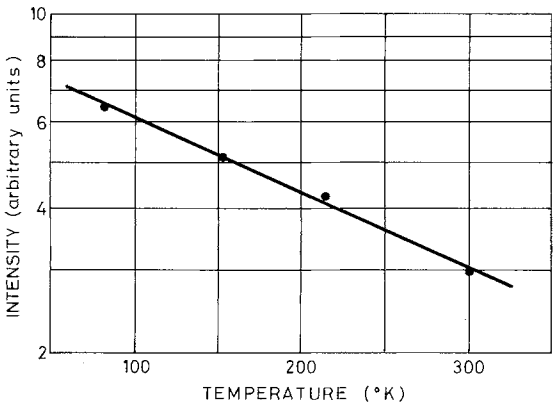

Fig. 3. Temperature dependence of the intensity of the *a*-Si spectrum

In Fig. 3 the temperature dependence of the spectral intensity is plotted on a logaritmic scale. The dependence is seen to be linear, in agreement with the assumption that all components of the *a*-spectrum have the same temperature dependence. The high-temperature Debye approximation can then be applied to find a Debye temperature for the *a*-spectra [11]:

$$f(T) = \exp(-6E_R T/k_B\theta_D^2), \quad T \gtrsim \tfrac{1}{2}\cdot\theta_D. \quad (2)$$

where $f(T)$ is the Debye-Waller factor at temperature T. The θ_D's thus deduced are listed in Table 2 and were found to coincide with the values for the *c*-spectra, when the same method of calculation is employed [3]. An evaluation of the absolute intensity of the *a*-Si spectrum as compared to that of the *c*-Si spectrum reveals that within an experimental uncertainty of 5% these are also equal.

In the case of amorphous germanium, measurements have only been made at room temperature and 77 K. The results are qualitatively the same as for amorphous silicon. No temperature-dependent variation in the shape of the *a*-Ge spectrum was observed and the Debye-Waller factors were not measurably different from the *c*-Ge values.

C. Dose and Temperature Dependence of the Amorphization of Silicon by Sn Implantations

Room-temperature implantations of Sn into silicon single crystals at doses $\lesssim 2\cdot 10^{13}\,Sn/cm^2$ yielded a spectrum that, within experimental error, was not different from the *c*-Si spectrum. Previous channel-

ing measurements [7] on samples implanted with $\sim 10^{13}$ Sn/cm^2 showed a significant amount of disorder in the implanted layer, but this apparently has no influence on the microscopic surroundings of the Sn atom. For doses from $\sim 10^{14}$ Sn/cm^2 to $\sim 10^{16}$ Sn/cm^2, the typical *a*-Si spectrum was observed, and there was no measurable dose dependence. For implantations of 10^{15} Sn/cm^2 at 250 °C, and up to $\sim 2 \cdot 10^{15}$ Sn/cm^2 at 450 °C, the *c*-Si spectrum was also observed.

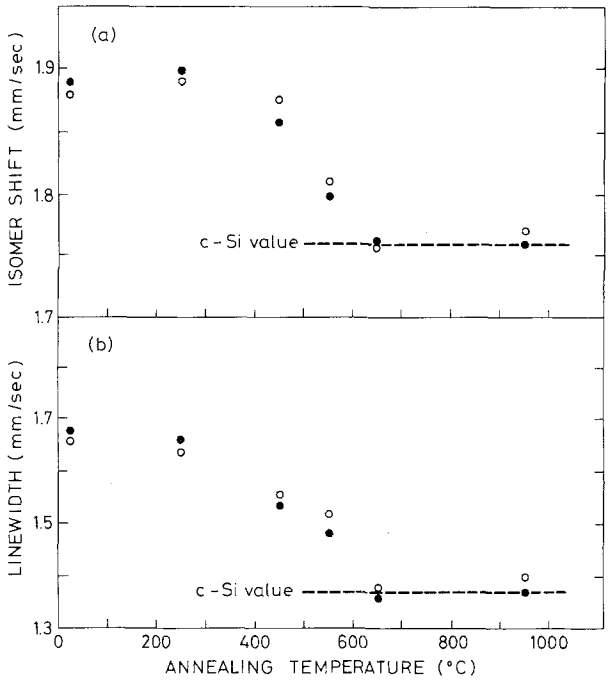

Fig. 4a and b. Variation of the average isomer shift **a** and halfwidth **b** of the spectra from two amorphized silicon samples upon stepwise annealing, ●=Si⟨111⟩ implanted with 10^{15} Sn/cm^2, ○=Si⟨100⟩ implanted with 10^{15} Sn/cm^2

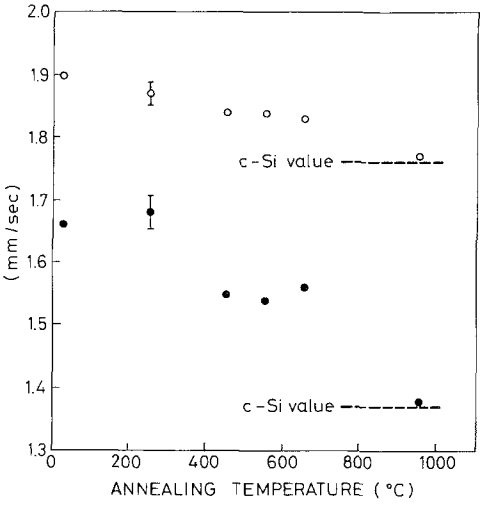

Fig. 5. Variation of the average isomer shift (○) and halfwidth (●) upon annealing of a Si⟨111⟩ sample implanted at room temperature with $5 \cdot 10^{14}$ Sn/cm^2 and $5 \cdot 10^{15}$ ^{16}O/cm^2

D. Annealing Experiments on Silicon and Germanium Samples

Two silicon crystals, cut perpendicular to the ⟨100⟩ and ⟨111⟩ directions, were implanted at room temperature with 10^{15} Sn/cm^2 (samples Si1 and Si10, respectively in Table 1) and measured at room temperature after 20-min isochronal anneal steps of 100 °C from 250 °C to 950 °C. The variation of the average isomer shift and linewidth of the spectra as a function of annealing temperature are displayed in Fig. 4a and b, respectively. No modifications are

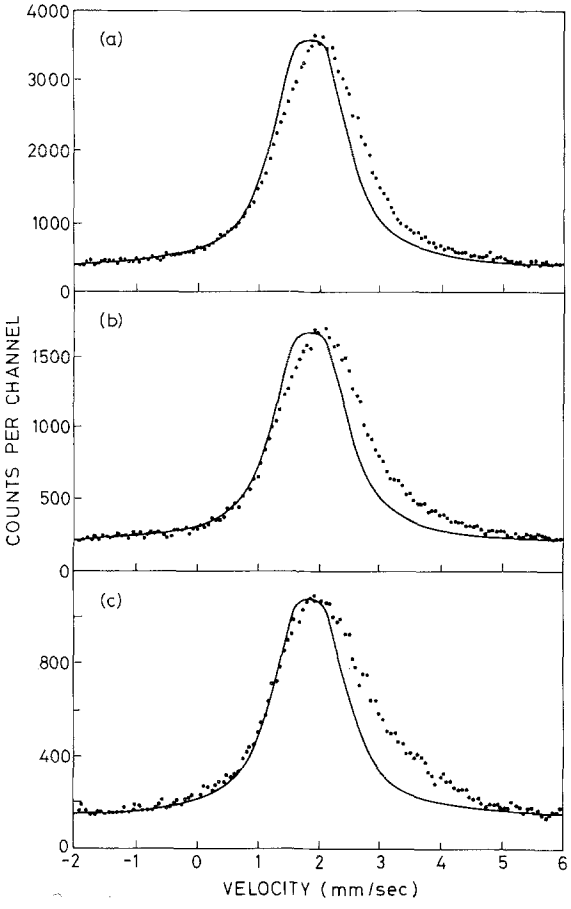

Fig. 6a–c. Mössbauer spectra (measured at liquid-nitrogen temperature, SnO_2 absorber) of three Si⟨111⟩ samples implanted at room temperature with 10^{16} Ne/cm^2 and post-implanted with $5 \cdot 10^{14}$ Sn/cm^2 at room temperature **a**, 250 °C **b**, and 350 °C **c**. The average isomer shifts are 1.99 ± 0.02, 2.04 ± 0.02, and 2.10 ± 0.02 mm/s, respectively, and the half-widths are 1.61 ± 0.03, 1.71 ± 0.03, and 1.83 ± 0.03 mm/s, respectively. The solid line represents the spectrum of Sn in crystalline silicon

Table 3. Results from inert-gas implanted Si samples

Sample	Implantation parameters				Anneal temp.	Measuring temp.	Spectrum	Line intensity in %				Type of substitutional component
	Sample temp.	Ion	Dose (cm^{-2})	Energy (keV)				I1.2	I1.76	I2.5	I3.4	
Kr(LN)	450 °C	^{119}Sn	$5 \cdot 10^{14}$	90		LN		–	100	–	–	*c*-Si
	LN	^{84}Kr	$8 \cdot 10^{15}$	90	RT	LN	Kr(LN, RT, LN)	–	100	–	–	*a*-Si
					950 °C	LN	Kr(LN, 950, LN)	0	85	12	3	*c*-Si
Kr(RT)	450 °C	^{119}Sn	$5 \cdot 10^{14}$	90		LN		–	100	–	–	*c*-Si
	RT	^{84}Kr	$8 \cdot 10^{15}$	90	RT	LN	Kr(RT, RT, LN)	–	100	–	–	*a*-Si
					950 °C	LN	Kr(RT, 950, LN)	0	65	30	5	– [a]
Ne(RT1)	450 °C	^{119}Sn	$5 \cdot 10^{14}$	90		LN		–	100	–	–	*c*-Si
	RT	^{20}Ne	$2 \cdot 10^{16}$	30	RT	LN	Ne(RT1, RT, LN)	–	100	–	–	*a*-Si
					250 °C							
					450 °C							
					550 °C							
					650 °C	LN	Ne(RT1, 650, LN)	5	67	12	8	*c*-Si [b]
Ne(RT2)	450 °C	^{119}Sn	$5 \cdot 10^{14}$	90		LN		–	100	–	–	*c*-Si
	RT	^{20}Ne	10^{16}	30	RT	LN	Ne(RT2, RT, LN)	–	100	–	–	*a*-Si
					– [c]	LN		–	100	–	–	*c*-Si
Ne(250)	RT	^{20}Ne	10^{16}	30								
	250 °C	^{119}Sn	$5 \cdot 10^{14}$	90	RT	LN	Ne(250, RT, LN)	2	83	13	2	*a*-Si
					550 °C							
					650 °C	LN	Ne(250, 650, LN)	16.0	58.7	11.0	14.3	*c*-Si
						RT	Ne(250, 650, RT)	9.8	66.8	11.0	12.4	*c*-Si
					950 °C	RT	Ne(250, 950, RT)	6.9	55.4	17.0	20.7	*c*-Si
Ne(350)	RT	^{20}Ne	10^{16}	30								
	350 °C	^{119}Sn	$5 \cdot 10^{14}$	90	RT	LN	Ne(350, RT, LN)	5	70	15	1	*a*-Si
					550 °C							
					650 °C	LN	Ne(350, 650, LN)	8.9	62.3	15.2	13.6	*c*-Si
						RT	Ne(350, 650, RT)	9.4	68.8	12.1	9.7	*c*-Si
					950 °C	LN	Ne(350, 950, LN)	6.2	61.5	21.1	11.2	*c*-Si
						RT	Ne(350, 950, RT)	6.2	70.8	13.1	9.9	*c*-Si

[a] very poor fit
[b] approximately 8% in SnO_2 line
[c] laser annealing $2 J/cm^2$

observed before 450 °C, where a very slight decrease in isomer shift and linewidth is seen. At 550 °C, the milky appearance typical of the amorphized area disappears almost completely for the ⟨110⟩ sample, whereas the ⟨111⟩ sample retains a reddish colour, indicating the presence of some residual disorder. A difference is not observed in the measured spectra. The decrease in isomer shift and linewidth proceeds more or less uniformly for the two samples and stabilizes at 650 °C, where the Mössbauer parameters of the *c*-Si spectrum are reached. At this temperature the implantation spots also disappear completely. Sample Si8, a Si ⟨111⟩ single crystal implanted at room temperature with $5 \cdot 10^{14}$ Sn/cm^2 plus $5 \cdot 10^{15}$ ^{16}O/cm^2, was annealed in the same manner. The results are shown in Fig. 6. It is seen that the *c*-Si values are not yet reached at 650 °C. For one-step anneals to 960 °C of samples Si3 and Si9 the *c*-Si spectrum was also observed.

A germanium sample implanted with 10^{15} Sn/cm^2 at room temperature, was annealed isochronally in 100 °C steps from 250 °C to 650 °C. The behaviour was qualitatively the same as for the silicon samples and the *c*-Ge spectrum was obtained after the 450 °C anneal.

E. Inert-Gas Implanted Samples

Several experiments were performed on high-dose, $\gtrsim 5 \cdot 10^{15}$ atoms/cm^2, inert-gas implanted Si ⟨111⟩ samples. These are compiled in Table 3. In our nomenclature, for example, Ne(250) represents an amorphized sample which is implanted with a high dose

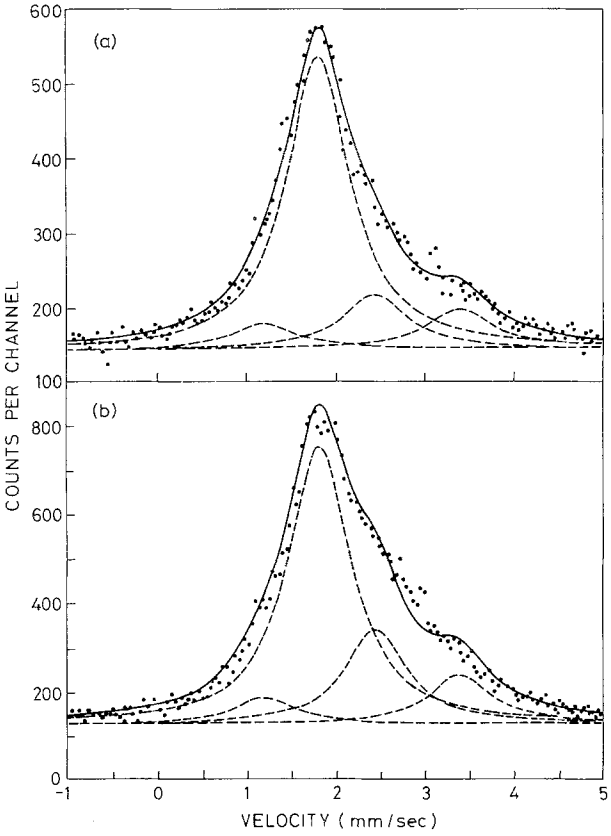

Fig. 7a and b. The Mössbauer spectra Ne(350, 950, RT) **a** and Ne(350, 950, LN) **b** measured with a $CaSnO_3$ absorber. The notation is given in Table 3

of Ne for which the final implant was performed at a sample temperature of 250 °C. The notation, for example Ne(250, 950, RT) represents the spectrum taken of sample Ne(250) annealed to 950 °C and measured at room temperature (LN corresponds to liquid-nitrogen temperature). In the left-hand side of Table 3 the implantation parameters are listed and in the right-hand side the further treatment of the samples is specified. To allow numerical comparison, the spectra have been fitted to four lines, the positions and linewidths of which were kept constant in the fits. The lines are denoted I1.2, I1.76, I2.5, and I3.4, where the "I" specifies that these lines occur in connection with high inert-gas concentrations and the number is the isomer shift at room temperature in mm/s. All lines are given natural linewidths in the fits. Lines with approximately the same isomer shifts have been observed previously for ^{119m}Te implantations into silicon (the ^{119m}Te decays via ^{119}Sb to ^{119}Sn, which is then measured by Mössbauer spectroscopy [5]). There is, however, no reason to assume that the positions of the lines and the defect structures assigned to these lines are identical to the ones observed here. The parameters of line I1.76 are chosen as such because a certain percentage of the implanted Sn atoms are expected to obtain a substitutional position during implantation and to retain this position during any subsequent post-implantations or annealing. In the last column of Table 3, it is stated whether a *c*-Si or an *a*-Si spectrum is observed. As all fits are made with respect to the *c*-Si line, no direct comparison can be made of the spectra containing the *a*-Si line to spectra containing only the *c*-Si line. Instead a comparison can be made of the two spectral parameters, the average isomer shift, and the linewidth. This has been done for the spectra of samples Ne(RT), Ne(250), and Ne(350) as shown in Fig. 6, where also the *c*-Si line is illustrated.

The choice of lines I1.2, I2.5, and I3.4 in the fitting procedure is based on the annealing series of samples Ne(250) and Ne(350). Figures 7a and b show examples of the observed spectra, where the individual intensities of the lines vary independently with the measuring temperature. The moderately enriched (50%) $CaSnO_3$-absorber material used here gives relatively good resolution, but also poor statistics. The isomer shifts, linewidths, and relative intensities of the lines can therefore not be determined with any great certainty.

IV. Discussion

A. The Origin of the Difference in Shape Between c- and a-Spectra

From the experimental results presented in the preceeding section it is evident that the occurrence of *a*-spectra is correlated with the amorphous phase of the host materials and that these spectra deviate in a characteristic way from the *c*-spectra.

The difference in the appearance of the *c*-spectra and the *a*-spectra will be interpreted to result from small local deviations in the amorphous phase from ideal tetrahedral structure probably predominantly from bond bending effects. A substitutional Sn position is maintained in both cases. This interpretation will be substantiated in the following by evaluating those factors which otherwise were thought to modify the observed *a*-Si spectra:

a) Species independence. The *a*-Si spectrum appeared independent of the implanted species and their doses. Two types of species-dependent interactions may have been anticipated: either a direct interaction of the Sn atom with the impurities, resulting in Sn-impurity complexes, or an indirect interaction where the impurities trap defects and prevent their interaction with the Sn atom. Neither of these two possibilities have been observed.

Furthermore, for the implantation of 10^{16} Sn/cm^2, a high degree of supersaturation of Sn in silicon is obtained without precipitation of tin. Therefore it is concluded that the resulting Sn sites are determined by the interaction of Sn with the silicon host lattice.

b) Macroscopic defects. Amorphous layers produced by vapour deposition have large mass-deficient regions known as voids [12]. The number and size of these depend on the deposition conditions, and the void network is found to be diminished by ion implantations. Here both the deposition temperature and the implanted ion dose were varied without a corresponding variation in the *a*-spectra. Thus the *a*-spectrum seems to reflect a true microscopic property which is not particularly influenced by macroscopic fluctuations.

c) Defects in chemical bonding. The basic structure of amorphous silicon and germanium is generally accepted to be a continuous network where the covalent tetrahedral bonding is upheld, the stresses inherent in such a rigid but non-ideal tetrahedral network being relieved by some atoms having less than optimal coordination. The missing bonds are referred to as dangling bonds. The number of dangling-bond states in the amorphous phase is found to be at most of the order of one per 200 atoms of silicon [13]. Thus, unless the Sn atoms have a special affinity to dangling-bond sites, the fraction of Sn atoms in such sites is below the detection limit of ^{119m}Sn Mössbauer spectroscopy. In the case of crystalline silicon, strong experimental evidence has been given that Sn traps vacancies [13–16]. For implantations leading to amorphization it seems improbable that the Sn atoms occupy a significant number of dangling bond sites ($\gtrsim 5\%$), as these would be detectable by a lower Debye-Waller factor than the substitutional sites [4, 16]. The rupture of a bond means a marked decrease in the bonding forces and therefore a decrease in the Debye-Waller factor, which would give a difference in Debye temperature. This is, however, not observed.

d) Implantation-induced stress. On the basis that the implanted Sn atoms are located substitutionally in the amorphous host lattice, an isomer shift increase might originate from compressional stresses causing an increase in *s*-electron density at the nucleus of the Sn atom. The presence of large compressional stresses in implanted silicon layers has been reported by Eernisse [17], and these were found to be highly dose dependent. The average isomer shift of the *a*-spectra would therefore be expected to show a dose dependence as well. Specifically the spectrum of the low-dose (10^{14} Sn/cm^2) implanted silicon film, where implantation induced reorganization of the void network will also minimize the strain, should have a lower average isomer shift than samples implanted with 10^{16} Sn/cm^2. This is not observed.

One concludes that the Sn probe atoms are located substitutionally with four covalent bonds to their silicon neighbour atoms. The increase in isomer shift should then be due to deviations from an ideal tetrahedral structure in the microscopic local surroundings.

In the amorphous group-IV semiconductors such deviations occur in the form of bond bending or bond lengthening. For amorphous silicon and germanium it has been shown that the spread in bond angles is of the order of 10 degrees around the ideal value 109° 28′, whereas the energetically less favourable deviations in the form of bond lengthening are not observed to be more than 1% [18]. The possibility of a more significant bond lengthening around the heavy Sn impurity must, however, be considered. The valence electrons of substitutional Sn in crystalline group-IV semiconductors hybridize with the relevant orbitals of the neighbouring atoms of the host crystal and reproduce the host's electron configuration [2, 19]. This behaviour is reflected by an increase in isomer shift with increasing bond length of the host lattice (i.e., when going from diamond, silicon, germanium to α-tin), corresponding to an increase in *s*-electron density (and a decrease in *p*-electron density). This dehybridization correlates to a lowering of the bond strength with increasing atomic number. For Sn in the amorphous host lattice a direct decrease of the *p*-electron density in the bond to a neighbouring atom would therefore be expected to lead to a decrease in the bond strength and consequently a decrease in the Debye-Waller factor. Such an effect is not observed and the *a*-spectra have the same Debye-Waller factor independent of isomer shift. Thus it seems unlikely that bond lengthening around the Sn impurities plays any important role. Given that bond bending is the major factor determining the appearance of the *a*-spectra, it is concluded that as in the crystalline case the valence electrons of the Sn atom reproduce the electron configuration of the amorphous host as much as possible.

Since the Sn atom is a heavy impurity atom, its vibrational motion does not directly give information on the vibrational properties of the host lattice. Calculations of impurity motion in amorphous semiconductors as performed for crystalline materials [3] have not been attempted, but the vibrational density of states of amorphous silicon and germanium has been studied using several approaches [20–24]. These establish that there is a remarkable similarity between the vibrational density of states of

the crystalline and amorphous phases of silicon and germanium as a consequence of the fact that the short-range order of the crystalline form is essentially retained in the amorphous phase. Theoretical calculations by Yndurain and Sen [24] have shown the shape of the transverse peaks is insensitive to bond-angle variations, whereas the longitudinal modes are attenuated by short-range correlations such as the presence of closed rings of bonds. This is in accordance with the fact that the Debye-Waller factor is the same for ^{119}Sn embedded substitutionally in both crystalline and amorphous silicon and germanium, since the Debye-Waller factor is largely determined by the lowest frequency modes (in general $f \sim 1/\omega^2$, where ω is the phonon frequency), which correspond to the transverse acoustical peak [3].

The α-tin data suggest that it is likely that also this material can be amorphized, but nothing conclusive can be stated. The two different types of spectra, which are observed, may be due to slightly different material compositions (residual Hg content), which might influence the amorphization process and give different degrees of amorphization for otherwise identical implantation conditions. The fact that the shape of some α-tin spectra is so similar to that of *a*-silicon and *a*-germanium does, however, support the conclusion that the silicon atoms have no pronounced "impurity character" in the amorphous silicon and germanium hosts.

B. *Annealing Experiments*

The annealing experiments presented in Sect. III.4 do fall in line with the proposed interpretation of the *a*-Si and *a*-Ge spectra. The substitutional sites of the tin atoms are retained throughout the annealing sequences. The parameters of the Mössbauer spectra reflect a reordering of the host lattice as the microscopic surroundings of the tin atom obtain ideal tetrahedral symmetry. The progression towards the *c*-Si and *c*-Ge spectra is conditioned by the recrystallization of the amorphous phase. The gradual decrease in isomer shift and linewidth is therefore interpreted as an increasing contribution to the spectra from regions which have recrystallized, i.e., an increasing intensity in the *c*-Si line. For the annealing series of Sn-implanted samples (Fig. 4), the annealing is completed by 650 °C, whereas for the sample implanted with additionally $5 \cdot 10^{15}$ ^{16}O/cm^2 (Fig. 5), the recrystallization is well advanced but incomplete after the 650 °C anneal. Kennedy et al. [26] have shown that the regrowth rate was retarded by oxygen implantation. It is remarkable that no Sn-O interaction is indicated from the Mössbauer spectra. In two cases a reaction with high-dose implanted impurities has been observed: for high-dose (10^{16}/cm^2) Sn-implanted silicon, where an α-tin precipitation is observed [27], and for high-dose inert gas implanted samples, the behavior of which is discussed in the following section.

For the silicon single crystal implanted with hydrogen (sample Si7 in Table 1), the concentration of hydrogen atoms was 10%. The Mössbauer spectrum observed for this sample was the typical *a*-Si spectrum and it remained uneffected by annealing up to 250 °C. Also, no defect lines which could be related to the presence of hydrogen were observed for 10^{14} Sn/cm^2 implanted into a silicon film produced by the glow-discharge method*.

C. *Inert-Gas Implanted Samples*

The implantation and annealing behaviour of amorphous silicon layers containing high concentrations of inert gases has been extensively studied by transmission electron microscopy and Rutherford backscattering methods [28–30]. By studying the gas-bubble formation and the recrystallization process, these methods give evidence that the inert-gas atoms exhibit high diffusivity: around the track of the incident implanted ion, even for samples implanted at liquid nitrogen temperature; along extended defects formed in the expitaxially regrown layer; and along the grain boundaries in the polycrystalline layer. Normal atomic diffusion is only possible during high-temperature anneals ($\gtrsim$900 °C).

The high diffusivity of the inert-gas impurity atoms distinguish these experiments from the preceding ones. Qualitatively, the intensity of the new defect lines in the Mössbauer spectra can be correlated to an influence of this feature:

a) A comparison of the spectra of samples Ne(RT), Ne(250), and Ne(350) (Fig. 7) shows that the half-width and the average isomer shift increases with increasing implantation temperature. This corresponds to an increasing representation of lines I1.2, I2.5, and I3.4. For all room-temperature implanted samples, only the *a*-Si spectrum is observed, even when the inert-gas content is a high as $2 \cdot 10^{16}$ Ne/cm^2. Therefore the increasing representation of the defect lines with increasing post-implantation temperature may be the combined effect of an increasing diffusivity and an increasing probability of forming the defects in question.

b) Both the Kr(LN) and the Kr(RT) samples show

* Kindly supplied by M. Milleville, Marburg, FRG

the *a*-Si spectrum at room temperature. A one-step anneal to 950 °C gives a large percentage of defect lines in the sample Kr(RT), whereas the Kr(LN) sample shows an almost perfect substitutional reordering (~85% in the *c*-Si line). During both implantations the diffusivity of the inert-gas atoms is high enough to form bubbles, these being, however, larger and more numerous for the room-temperature implant which therefore should give a relatively larger retardation of the recrystallization process.

c) Upon annealing to 650 °C of the sample amorphized by $2 \cdot 10^{16}$ Ne/cm^2, a line having the characteristics of the SnO_2 line was observed at 0 mm/s. Such an oxidation of the Sn-probe atoms is interpreted as the result of blistering on the crystal surface due to the high Ne concentration.

An interpretation of the individual lines in the spectra is more ambiguous, the isomer-shift range covered by the defect lines corresponds to basically three different Sn-valence states: stannic (Sn^{4+}) for I1.2, covalent for I2.5, and stannous (Sn^{2+}) for I3.4 [31]. For I2.5, the most obvious interpretation would be that some dangling bonds have been formed. Simple calculations of the isomer shift increase upon the formation of dangling bonds correspond well with a resulting isomer shift of ~2.5 mm/s [4]. For lines I1.2 and I3.4 a more drastic change in bonding character must be assumed. Beta-tin has an isomer shift of ~2.57 mm/s, but it is improbable that β-tin precipitation is of significance here. Such precipitation has been observed upon annealing for doses of 10^{16} Sn/cm^2 [27], but for $\lesssim 10^{15}$ Sn/cm^2 no such effect was observed for the other annealed samples, i.e., Si1, Si8, and Si10. Also for hot implantations, even at 450 °C and a dose of $2 \cdot 10^{15}$ Sn/cm^2 solely the *c*-Si line is observed.

Upon laser annealing of sample Ne(RT2), only the *c*-Si spectrum is observed. This rapid annealing form does apparently not allow the formation of the complex defects otherwise observed.

V. Summary

For room-temperature implantations of the ^{119m}Sn Mössbauer atoms into amorphized samples of silicon, germanium, and α-tin, spectra are observed, which are concluded to be characteristic of the microstructure of the amorphous phases of these materials. The *a*-Si and *a*-Ge spectra are very similar in that they have the same shape and deviate in the same manner from the spectra of ^{119}Sn in the corresponding crystalline material. The individual lines of an *a*-spectrum have the same temperature dependence so that a characteristic Debye temperature can be calculated for tin in the amorphous material. This Debye temperature is the same as for tin in the corresponding crystalline material. The tin atoms are proposed to assume substitutional positions with bonding structures that resemble those of the host atoms. The present results are in agreeement with the current picture of amorphous silicon and germanium: on a microscopic scale these materials are found to be very much alike and the vibrational properties which determine the Debye temperature, are primarily governed by the nearest-neighbour interactions.

Upon annealing of the amorphous samples, differences are observed which depend on the implanted species and doses. Specifically, defects are formed for high-dose inert-gas implanted samples.

We would like to thank J. Chevallier and H.L. Nielsen for technical support, N.E. Holm and A.N. Larsen for experimental help, and E. Antoncik for useful discussions.
This work has been supported by the Danish Natural Science Research Council.

References

1. Adler, D.: Amorphous semiconductors. (Butterworths, London: Chemical Rubber Co. 1972)
2. Weyer, G., Nylandsted Larsen, A., Deutch, B.I., Andersen, J.U., Antoncik, E.: Hyperfine Interact. **1**, 93 (1975)
3. Petersen, J.W., Nielsen, O.H., Weyer, G., Antoncik, E., Damgaard, S.: Phys. Rev. B **21**, 4292 (1980)
4. Weyer, G., Nylandsted Larsen, A., Holm, N.E., Nielsen, H.L.: Phys. Rev. B **21**, 4939 (1980)
5. Nylandsted Larsen, A., Weyer, G., Nanver, L.K.: Phys. Rev. B **21**, 4951 (1980)
6. Coey, J.M.D.: J. Phys. (Paris) **35**, C6-89 (1974)
7. Weyer, G., Andersen, J.U., Deutch, B.I., Golovchenko, J.A., Nylandsted Larsen, A.: Radiat. Eff. **24**, 117 (1974)
8. Van Lent, P.H.: Acta Metall. **10**, 1089 (1962)
9. Weyer, G.: Moessbauer Eff. Methodol. **10**, 301 (1976)
10. Mayer, J.W., Eriksson, L., Picraux, S.T., Davis, J.A.: Can. J. Phys. **46**, 668 (1968)
11. Wegener, H.: Der Mössbauer Effekt. Mannheim: Bibliographisches Institut 1966
12. Ohdomari, I., Ikeda, M., Yoshimoto, H., Onoda, N., Tanabe, Y., Itoh, T.: Ion implantation in semiconductors. Chernow, F., Borders, J.A., Brice, D.K. (eds.). p. 49. New York; London: Plenum Press 1976
13. Thomas, P.A., Brodsky, M.H., Kaplan, D., Lepine, D.: Phys. Rev. B **18**, 3059 (1978)
14. Brelot, A.: Annu. Conf. Nucl. and Space Radiat. Eff., Univ. of Washington. IEEE Nucl. Sci., p. 220 (1972)
15. Watkins, G.D.: Phys. Rev. B **12**, 4388 (1975)
16. Damgaard, S., Petersen, J.W., Weyer, G.: Hyperfine Interact. **10**, 751 (1981)
17. Eernisse, E.P.: Appl. Phys. Lett. **18**, 518 (1971)
18. Alben, R., Weaire, D., Smith, J.E., Brodsky, M.H.: Phys. Rev. B **11**, 2271 (1975)
19. Antoncik, E.: Phys. Status Solidi (*b*) **79**, 605 (1977)
20. Lannin, J.S.: Solid State Commun. **12**, 947 (1973)
21. Brodsky, M.H., Lurio, A.: Phys. Rev. B **9**, 1646 (1974)

22. Axe, J.D., Keating, D.T., Cargill, III, G.S., Alben, R.: Tetrahedrally bonded amorphous semiconductors. Brodsky, M.H., Kirkpatrick, S., Weaire, D. (eds.). p. 279. New York: AIP 1974
23. Weaire, D., Alben, R.: J. Phys. C **7**, L189 (1974)
24. Yndurain, F., Sen, P.N.: Phys. Rev. B **14**, 513 (1976)
25. Dearnaley, G., Freeman, J.H., Nelson, R.S., Stephen, J.: Ion Implantation. p. 122. Amsterdam: North-Holland 1973
26. Pronko, P.P., Rechtin, M.D., Foti, G., Csepregi, L., Kennedy, E.F., Meyer, J.W., Sigmon, T.W.: Ref. 12, p. 503
27. Nanver, L.K., Weyer, G., Deutch, B.I.: Phys. Status Solid (a) **61**, K29 (1980)
28. Revesz, P., Wittmer, M., Roth, J., Mayer, J.W.: J. Appl. Phys. **49**, 5199 (1978)
29. Wittmer, M., Roth, J., Revesz, P., Mayer, J.W.: J. Appl. Phys. **49**, 5207 (1978)
30. Cullis, A.O., Seidel, T.E., Meek, R.L.: J. Appl. Phys. **49**, 5188 (1978)
31. Lees, J.I., Flynn, P.A.: J. Chem. Phys. **48**, 882 (1968)

L.K. Nanver
G. Weyer
B.I. Deutch
Institute of Physics
University of Aarhus
DK-8000 Aarhus C
Denmark